Predicting atomic diffusion in concentrated magnetic alloys: The case of paramagnetic Fe-Ni

Kangming Li ⬤, Chu-Chun Fu ⬤, Maylise Nastar, and Frédéric Soisson ⬤

Université Paris-Saclay, CEA, Service de recherche en Corrosion et Comportement des Matériaux, SRMP, F-91191 Gif-sur-Yvette, France

Predicting atomic diffusion in concentrated magnetic systems is challenging due to thermal magnetic effects and complex magnetochemical interplay. We propose an efficient approach via kinetic Monte Carlo using *ab initio* parametrized models. We demonstrate its accuracy in the case of Fe-Ni alloys, where we successfully predict and explain the weak composition dependence of diffusion coefficients due to a compensation of distinct contributions of their constituents. The diffusion-behavior difference between the paramagnetic and the magnetic ground states is elucidated, evidencing the role of magnetic disorder.

I. INTRODUCTION

Thermodynamic and kinetic properties of pure and multicomponent magnetic systems are known to be strongly influenced by magnetic ordering, excitation, and transition, as well as the interplay with other degrees of freedom [1–8]. However, the treatment of finite-temperature magnetism and magnetochemical coupling remains a major bottleneck for an accurate prediction of thermodynamic and kinetic properties in magnetic alloys. This is indeed the case for atomic diffusion, a fundamental process governing the kinetics of microstructural evolutions such as segregation, precipitation, and phase ordering [9–13]. Despite its importance for kinetic simulations in magnetic alloys, so far a proper inclusion of finite-temperature magnetic effects in the modeling of atomic diffusion remains an open issue for systems beyond the dilute limit.

Indeed, previous theoretical investigations of diffusion properties were typically performed for nonmagnetic systems, using classical molecular dynamics (MD) or kinetic Monte Carlo (MC) simulations to follow the trajectories of atomic movements [14–20], or using semianalytical diffusion models with a limited number of jump frequencies as input data [21–28]. For magnetic systems, however, these methods are unable to explicitly account for the magnetic degree of freedom and thermal magnetic effects.

Recently, various approaches have been developed to treat the finite-temperature magnetism for diffusion, either by interpolating the density functional theory (DFT) results between the magnetic ground state and the perfectly paramagnetic (PM) state modeled by the disordered local moment (DLM) method [29–31], or by applying either effective interaction models (EIMs) or spin-lattice potentials containing explicit atomic and spin variables in MC or MD simulations [32–35]. These studies have so far been restricted to the case of infinitely dilute Fe-*X* alloys [29–35], whereas such a kinetic modeling remains elusive for magnetic alloys beyond the dilute limit. The latter is important not only because of the practical interest associated with nondilute alloys, but also because of potentially new physics that may emerge due to a composition dependence of the magnetochemical coupling.

Indeed, the major challenge of a kinetic modeling for concentrated magnetic alloys is an accurate and efficient treatment of the complex magnetochemical interplay. In the infinitely dilute case, various magnetic configurations only need to be sampled for a very small number of local chemical environments. By contrast, in a concentrated alloy, it is necessary to sample a much larger number of local chemical environments, and of magnetic configurations for each of the chemical ones due to their mutual dependence [2,36]. With a purely DFT approach, it is practically impossible to determine migration barriers for such a huge number of local chemical and magnetic environments encountered during the diffusion, due to the prohibitively high computational cost. Furthermore, there is no available semianalytical model allowing to link the DFT-calculated migration barriers to macroscopic transport coefficients in a concentrated alloy. Though spin-lattice MD simulations enable a natural account for the interplay between magnon, phonon, and chemical effects, it is still highly challenging to develop sufficiently accurate spin-lattice potentials for the whole magnetochemical phase diagram [37]. In addition, spin-lattice MD simulations are computationally inefficient for thermally activated processes such as vacancy-mediated diffusion in alloys, except for very high temperatures.

In this work, we propose a modeling approach representing a good compromise between accuracy and efficiency for kinetic properties in concentrated magnetic alloys. Our approach combines kinetic MC simulations with DFT-parametrized effective interaction models. We demonstrate its ability by applying it to the face-centered-cubic (fcc) Fe-Ni alloys, a model system of austenitic alloys. For this system, there are a few experimental tracer diffusion data but available only in the high-temperature PM solid solutions [38,39]. In previous theoretical studies of this system, however, the effects of magnetic excitation and transition were neglected [40–44]. Furthermore, the experimental Fe and Ni diffusion coefficients (D_{Fe}^* and D_{Ni}^*, respectively) show a weak composition dependence (Fig. 1), whereas previous MD and MC modelings predicted that D_{Fe}^* varies by more than three orders of magnitude between pure Fe and pure Ni [42–44]. For the Fe-Ni alloys, we aim to solve this experimental-theoretical
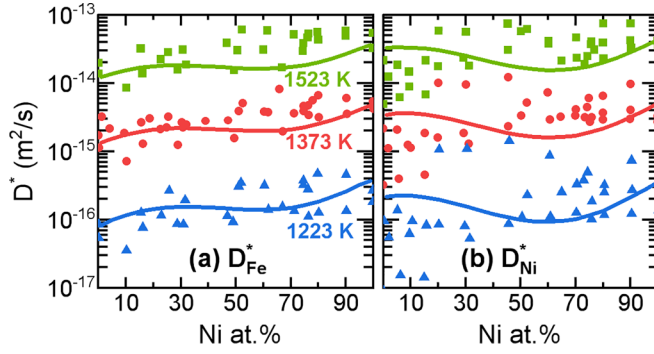
FIG. 1. Tracer diffusion coefficients in PM fcc Fe-Ni alloys under equilibrium conditions. Lines represent the predictions from this work. Symbols are the experimental data compiled in Ref. [38], including 10 different studies in nondilute alloys (only two of them measured simultaneously, D_{Fe}^* and D_{Ni}^*).

discrepancy on the composition dependence via determination of the tracer diffusion coefficients D^* and the composition evolution of the constituents of D^*, namely the equilibrium vacancy concentrations $x_{\text{V,eq}}$, the jump frequencies Γ, the kinetic correlation factors f, and the atom-vacancy binding. We also discuss the impact of magnetic disorder on these quantities, as well as the diffusion properties in out-of-equilibrium conditions.

II. METHODS

A. Effective interaction model

Our approach follows a similar principle to those used in the studies of Cu and Mn solute diffusion in bcc Fe [31,32], namely using on-lattice MC simulations coupled with a DFT-parametrized EIM. The present EIM goes beyond our previous on-lattice model of fcc Fe-Ni alloys [36,45] by including a description of the saddle-point (SP) configurations for vacancy-mediated diffusion as follows. An N-site saddle-point configuration consists of one SP atom, $N-2$ on-lattice (OL) atoms, and two first-nearest-neighbor (1NN) vacant sites. We express the total energy of the SP configuration as the sum of two parts:

$$E_{\text{tot}} = E_{\text{OL}} + E_{\text{SP}}, \tag{1}$$

where E_{OL} is the total energy of the on-lattice system determined from our previous model [36,45], and E_{SP} is the energy due to the interactions of the SP atom with its OL neighboring atoms parametrized in this work.

For the on-lattice system, E_{OL} has the following form:

$$E = \sum_i \sigma_i \left(A_i M_i^2 + B_i M_i^4 + \sum_j \sigma_j J_{ij} \boldsymbol{M}_i \boldsymbol{M}_j \right)$$
$$+ \sum_i \sigma_i \left(\epsilon_i + \sum_j \sigma_j V_{ij} \right), \tag{2}$$

where σ_i is the occupation variable; $\boldsymbol{M}_i$ is the magnetic moment; A_i, B_i, and J_{ij} are the magnetic on-site and exchange-coupling parameters; $\sum_j$ is a sum over all the neighboring atoms within the fourth nearest-neighbor shell; and ϵ_i and V_{ij}

are the chemical on-site and pair-interaction parameters. Our EIM for the on-lattice system has been shown to correctly predict the magnetochemical phase diagram and the equilibrium vacancy concentration in fcc Fe-Ni alloys [36,45,46]. The relevant model parameters can be found in [36].

We express E_{SP} as follows:

$$E_{\text{SP}} = A_{\text{SP}} M_{\text{SP}}^2 + B_{\text{SP}} M_{\text{SP}}^4 + \sum_j J_{\text{SP},j} \boldsymbol{M}_{\text{SP}} \boldsymbol{M}_j$$
$$+ \epsilon_{\text{SP}} + \sum_j V_{\text{SP},j}, \tag{3}$$

where M_{SP} is the magnetic moment of the saddle-point atom, and A_{SP}, B_{SP}, $J_{\text{SP},j}$, ϵ_{SP}, and $V_{\text{SP},j}$ are the corresponding magnetic and nonmagnetic parameters. The sum $\sum_j$ goes over the atoms within the fourth-neighbor shell of the SP atom. Note that the number of neighbors and the distance from neighbors for the SP atom are different from those of the OL atoms.

The EIM is fitted to about 1400 DFT energy data involving magnetically and chemically ordered and disordered structures. There is no fitting on experimental data. While the lattice vibration effects on phase stability are included in the EIM [36,46], vacancy formation vibrational entropies S_f^{vib} and attempt frequencies of atom-vacancy exchanges ($\Gamma_{0,\text{Fe}}$ and $\Gamma_{0,\text{Ni}}$) in the alloys are not intrinsically accounted for in the EIM. Instead, they are linearly interpolated from the DFT values in antiferromagnetic double-layer (AFD) Fe ($S_f^{\text{vib}} = 3.1k_B$, $\Gamma_{0,\text{Fe}} = 1.9$ THz, $\Gamma_{0,\text{Ni}} = 24.3$ THz) and in FM Ni ($S_f^{\text{vib}} = 2.2k_B$, $\Gamma_{0,\text{Fe}} = 3.8$ THz, $\Gamma_{0,\text{Ni}} = 22.2$ THz) [47]. Magnon-phonon coupling [7,48,49] is not considered.

B. Kinetic Monte Carlo simulations

The EIM is used in canonical MC simulations in a 16 384-site fcc lattice. The vacancy-free system is first relaxed according to the METROPOLIS algorithm to ensure that both the magnetic and chemical configurations are in thermal equilibrium at the given temperature. Next, a vacancy is introduced into the system by removing a randomly selected atom. The atomic diffusion is then simulated by exchanging the vacancy with one of its 1NN atoms. Each vacancy-atom exchange and the corresponding time increment are obtained by using the residence time algorithm [15]:

(i) Calculate the migration barrier $E_{m,i}$ for each 1NN atom i of the vacancy. Please note that $E_{m,i}$ is dependent on the local chemical and magnetic environments.

(ii) Calculate the jump frequency $\Gamma_i = \Gamma_{i,0} \exp(-\frac{E_{m,i}}{k_B T})$, where $\Gamma_{i,0}$ is the attempt frequency of the atom i. Then, calculate the cumulative jump frequency $\Gamma_i^{\text{cumu}} = \sum_{j=1}^i \Gamma_j$.

(iii) Draw a uniform random variable u in the interval $[0, \Gamma_{12}^{\text{cumu}})$. If u is in the interval $[\Gamma_{i-1}^{\text{cumu}}, \Gamma_i^{\text{cumu}})$, exchange the vacancy with the atom i.

(iv) Update the time $t_{\text{MC}} = t_{\text{MC}} + 1/\Gamma_{12}^{\text{cumu}}$.

We note that the magnetic configuration is relaxed again after each vacancy-atom exchange to ensure that the magnetic configuration is in thermal equilibrium at the given temperature before the next vacancy-atom exchange.

Via this kinetic MC approach, we determine the tracer diffusion coefficients D_A^* ($A =$ Fe or Ni) from the Einstein

relation [12]:

$$D_A^* = \frac{\langle r_A^2 \rangle}{6t}, \tag{4}$$

where $\langle r_A^2 \rangle$ is the mean-square displacement of tracer atoms. Here all atoms of the same element A are considered as tracers to enhance statistics [32,40–44]. In Eq. (4), t is the physical time obtained as [15,16]

$$t = t_{MC} \frac{x_{V,MC}}{x_V}. \tag{5}$$

Here t_{MC} is the simulated time, $x_{V,MC} = 1/N_{site}$ is the simulated vacancy concentration, and x_V is the vacancy concentration in a real system. For diffusion under thermal equilibrium, we use the equilibrium vacancy concentration $x_{V,eq} = \exp(-G_f/k_B T)$, with the vacancy formation free energy $G_f = G_f^{mag} - T S_f^{vib}$, where G_f^{mag} is the vacancy formation magnetic free energy computed from MC simulations using a Widom-type scheme [36,45].

III. RESULTS AND DISCUSSION

A. Comparison with experimental tracer diffusion coefficients

The highest Curie temperature of fcc Fe-Ni solid solutions is predicted to be 880 K at Fe-67%Ni [36], in good agreement with experimental data [50,51]. The experimental tracer diffusion coefficients in these alloys are available only in the PM regime. As shown in Fig. 1, the experimental data suggest a weak composition dependence of the diffusion coefficients considering the data dispersion. Our predicted values are in overall quantitative agreement with the experimental data, showing that the largest variation of D^* in the whole composition range is around a factor of 4 at 1223 K and a factor of 3 at 1523 K. For all the studied temperatures, the minima of D_{Fe}^* and D_{Ni}^* occur in fcc Fe and Fe-60%Ni, respectively.

It is worth noting that previous simulation results in concentrated Fe-Ni [41–44] and other alloy systems [17–20] were often calculated with arbitrarily fixed vacancy concentrations and did not consider the composition evolution of the equilibrium vacancy concentration. Hence a direct comparison with available experimental diffusion coefficients measured under equilibrium conditions as shown in Fig. 1 is often missing in the literature.

B. Constituents of diffusion coefficients

1. Composition dependence of constituents of diffusion coefficients

The composition dependence of the diffusion coefficients can be better understood via a decomposition into its constituents. First of all, in an infinitely dilute alloy, the solute-diffusion coefficient is known to have the following expression [12,21,22]:

$$D_A^* = a^2 f_A x_{V,eq} \exp\left(\frac{G_b^{V-A}}{k_B T}\right) \Gamma_A, \tag{6}$$

where a is the lattice constant, f_A is the correlation factor for the solute atom A, $x_{V,eq}$ is the equilibrium vacancy concentration, G_b^{V-A} is the solute-vacancy binding free energy, and Γ_A is the jump frequency of the solute atom.

To derive a formally equivalent expression for concentrated alloys, we first recall the expressions for the kinetic correlation factor f_A [12] and the Cowley-Warren short-range order parameter of 1NN vacancy-A pairs α_{V-A}^{1NN} [52,53]:

$$f_A = \frac{\langle r_A^2 \rangle}{n_A\, d^2}, \tag{7}$$

$$\alpha_{V-A}^{1NN} = 1 - \frac{x_A^V}{x_A}, \tag{8}$$

where n_A is the average number of jumps per A atom during t_{MC}, d is the jump length equal to the 1NN distance ($= a/\sqrt{2}$ in an fcc lattice), x_A^V is the average concentration of A in the 1NN shell of the vacancy, and x_A is the nominal concentration of A atoms in the system. To derive the expression of the effective jump frequency for A atoms (Γ_A) in an alloy, we first recall Γ_A in the case of a pure system of A atoms [12]:

$$\Gamma_A = \frac{N_{jump}}{z\, t_{MC}}, \tag{9}$$

where N_{jump} is the total performed atomic jumps during the time interval t_{MC}, and z is the 1NN coordination number (equal to 12 in an fcc lattice). In an alloy, N_{jump} becomes the total number of jumps of A atoms (namely $n_A N_A$, with N_A the number of A atoms), and z becomes the average number of 1NN A atoms around the vacancy (namely $z x_A^V$). Therefore, in the alloy,

$$\Gamma_A = \frac{n_A N_A}{z\, x_A^V\, t_{MC}}. \tag{10}$$

Combining Eqs. (7)–(10), we have

$$a^2 f_A x_{V,MC} \left(1 - \alpha_{V-A}^{1NN}\right) \Gamma_A = \frac{\langle r_A^2 \rangle}{6\, t_{MC}}. \tag{11}$$

Using the Einstein relation [12], we arrive at the following expression:

$$D_A^* = a^2 f_A x_{V,eq} \left(1 - \alpha_{V-A}^{1NN}\right) \Gamma_A. \tag{12}$$

We note that $1-\alpha_{V-A}^{1NN}$ becomes $\exp(G_b^{V-A}/k_B T)$ in Eq. (6) in an infinitely dilute alloy.

As shown in Fig. 2, the composition dependence of D^* and of its main constituents ($x_{V,eq}$, Γ, and f) can be qualitatively different. Although D_{Fe}^* and D_{Ni}^* show a weak composition dependence, their constituents can have a distinct behavior. In particular, $x_{V,eq}$ varies with composition by up to a factor of 8, which is mainly related to the large difference between the vacancy formation energies in Fe and Ni (1.8 and 1.4 eV, respectively [36]). The impact of $x_{V,eq}$ on the composition dependence of D^* is partially compensated by the other constituents, especially the effective jump frequency, while the effects of f and $1 - \alpha^{1NN}$ are minor (Table I). Specifically, the variation of D_{Fe}^* is mainly dictated by the behavior of $x_{V,eq}$, both presenting a minimum in pure Fe and a maximum in pure Ni. On the other hand, the variation of D_{Ni}^* mainly results from an interplay of $x_{V,eq}$ and Γ_{Ni}, which have an opposite composition dependence.
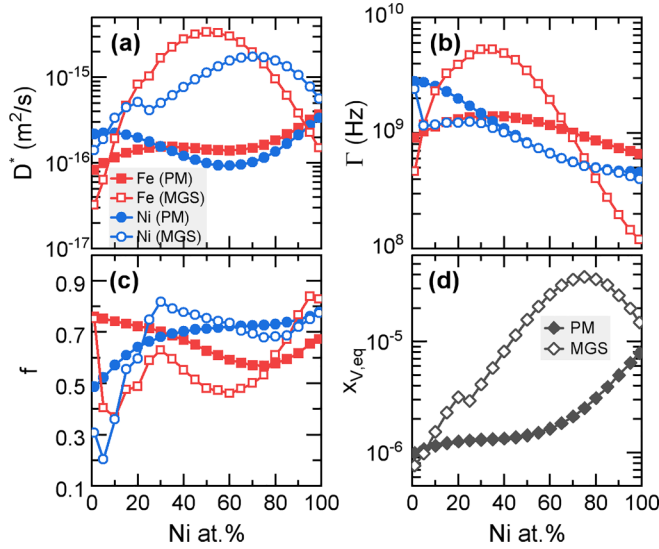
FIG. 2. Calculated (a) tracer diffusion coefficients, (b) effective jump frequencies, (c) kinetic correlation factors, and (d) equilibrium vacancy concentrations vs Ni content at 1223 K. The composition dependence for other temperatures in the PM regime (above 1000 K) is similar. The y-axis in (a),(b),(d) and in (c) adopt, respectively, a log and a linear scale.

2. Temperature dependence of the effective atomic jump frequency

The effective atomic jump frequency is usually expressed as

$$\Gamma_A = \Gamma_{0,A} \exp\left(-\frac{E_{m,A}}{k_B T}\right),\tag{13}$$

where $E_{m,A}$ is the effective migration energy for A atoms. Often $E_{m,A}$ is assumed to be a constant and Γ_A is assumed to follow an Arrhenius law, for instance in pure systems and dilute alloys [22,26,41]. However, although the systems are rather simple, the presence of magnetic order-disorder transitions may lead to a non-Arrhenius behavior [31,32,54]. Here we intend to discuss whether there is a deviation from this often assumed Arrhenius law in concentrated PM Fe-Ni alloys.

First, it should be pointed out that in principle $E_{m,A}$ is temperature-dependent even for a nonmagnetic alloy, since $E_{m,A}$ is an average of the exponentials of the individual migration energies $E_{m,A}^i$, which depend on local chemical configuration i. For magnetic systems, as magnon excitations are faster than atomic jumps [32], each individual migration

energy $E_{m,A}^i$ is actually a migration magnetic free energy $G_{m,A}^i$ as it integrates fast magnetic degrees of freedom (i.e., averaged over various magnetic configurations j of a given chemical configuration i). In bcc Fe, for instance, the Fe migration magnetic free energy is known to vary significantly with magnetic order and thus with temperature [32].

In magnetic alloys, $E_{m,A}$ becomes the effective migration magnetic free energy $G_{m,A}$, and it can depend on both magnetic and chemical orders. According to our EIM, the Fe-Ni alloys are the PM disordered solid solutions above 900 K for the whole composition range. For the temperature range discussed in this work (1223–1523 K), the variations of $E_{m,\mathrm{Fe}}$ and $E_{m,\mathrm{Ni}}$ with temperature are found to be small (less than 0.03 eV, which is within the typical calculation uncertainties). As a result, we find that the temperature dependence of Γ_{Fe} and Γ_{Ni} is well described by the Arrhenius law in the considered temperature range.

C. Impact of magnetic state on diffusion properties

It should be noted that previous state-of-the-art simulations in concentrated magnetic alloys did not consider magnetic excitation. First-principles calculations in magnetic alloys typically use a magnetic ground state (MGS) at 0 K to represent the equilibrium magnetic state at finite temperatures, which is only valid if the effects of magnetic disorder on diffusion properties are negligible. To elucidate the role of magnetic disorder, we also show in Fig. 2 the diffusion coefficients and their main constituents in the solid solutions at the corresponding 0 K magnetic configuration (MGS). In the MC simulations, the paramagnetic (PM) configuration is obtained by equilibrating the chemical and magnetic degrees of freedom at a given temperature T. By contrast, the MGS is simulated by applying the 0 K magnetic structures to the chemical equilibrium configurations at T. For the solid solutions with more than 20%Ni, the predicted MGS is collinear ferromagnetic (FM). Below 20%Ni, the MGS gradually becomes noncollinear with decreasing Ni content, with the reduced magnetization decreasing to zero at 5%Ni [36]. For pure fcc Fe, the MGS is predicted to be a spin spiral with $\mathbf{q} = \frac{2\pi}{a}(0, 0, 0.3)$ [45].

We note a significant PM-MGS difference in both D_{Fe}^* and D_{Ni}^* in concentrated regions, which is mainly due to the large difference of vacancy concentration around 60–80 %Ni. The significantly larger equilibrium vacancy concentration in the MGS is related to the strong FM interaction in the concentrated alloys, as shown in Ref. [36]. To verify the EIM results, we also checked with DFT for the case of the $L1_2 - \mathrm{FeNi_3}$ structure and confirmed an increase in vacancy formation energy due to the magnetic disorder [36].

Concerning the Fe diffusion, the effective jump frequency Γ_{Fe} is another important factor leading to the large MGS-PM difference in D_{Fe}^*. While the composition evolution of Γ_{Fe} is qualitatively similar between the PM and MGS, the amplitude of the variation is much more significant in the MGS: in the whole composition range, Γ_{Fe} changes by up to a factor of 43 in the MGS, whereas it varies by no more than a factor of 2 in the PM state. This result indicates a reduction of chemical-composition effects due to magnetic disorder, which is not only seen in Γ_{Fe} but is also observed in
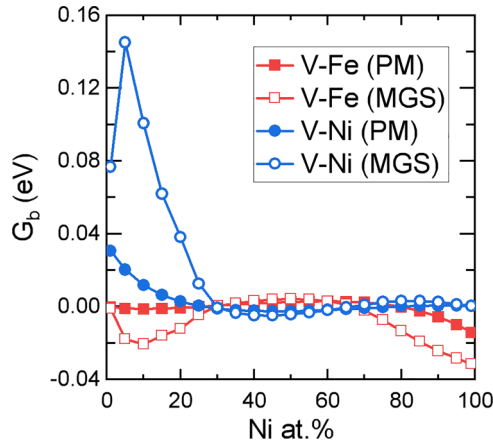
TABLE I. Maxima and minima of $x_{\mathrm{V,eq}}$ (in 10^{-6}), Γ_A (in GHz), f_A, $1 - \alpha_{\mathrm{V-A}}^{\mathrm{1NN}}$, and D_A^* (in 10^{-6} m^2/s) in PM Fe-Ni solid solutions at 1223 K. Please note that $x_{\mathrm{V,eq}}$ is independent of the diffusing element A, therefore its extremum is the same for Fe and Ni.

	$x_{\mathrm{V,eq}}$	Γ_A	f_A	$1-\alpha_{\mathrm{V-A}}^{\mathrm{1NN}}$	D_A^*
Max ($A = $ Fe)	8.0	1.4	0.8	1.0	3.8
Min ($A = $ Fe)	1.0	0.7	0.6	0.9	0.8
Max ($A = $ Ni)	8.0	2.8	0.8	1.3	3.4
Min ($A = $ Ni)	1.0	0.5	0.5	1.0	0.9

FIG. 3. Generalized vacancy-atom 1NN binding free energy vs Ni concentration.

FIG. 4. Binding energy between the vacancy and a given Ni cluster in the AFD Fe vs the number of Ni atoms in the cluster.

the Fe and Ni diffusion coefficients, the equilibrium vacancy concentration, and the correlation factors (Fig. 2). A similar magnetic-disorder impact (reducing chemical-interaction effects) on the solute-vacancy binding and therefore on the solute and solvent migration barriers was also noted in dilute bcc Fe-Cu and Fe-Mn systems [31,32]. On the other hand, the effective jump frequency of Ni atoms is less affected by the magnetic state.

We find a very small value of f_{Fe} and f_{Ni} in the MGS around Fe-5%Ni. This is found to be related to the strong attraction between the vacancy and the small Ni clusters in an antiferromagnetic Fe lattice, which increases with the Ni-cluster size. To evidence this point, we first need to define a generalized 1NN vacancy-A binding free energy as

$$G_b^{V\text{-}A} = k_B T \ln\left(1 - \alpha_{V\text{-}A}^{1NN}\right) = k_B T \ln \frac{x_A^V}{x_A}. \qquad (14)$$

In the dilute limit ($x_A \to 0$), $G_b^{V\text{-}A}$ becomes the usual vacancy-solute binding free energy. The MC results of $G_b^{V\text{-}A}$ in the MGS and PM states are shown in Fig. 3. According to the definition of $G_b^{V\text{-}A}$, a positive value indicates that the 1NN A concentration around the vacancy is higher than the nominal x_A, namely an attraction of vacancy towards a Ni-rich environment. Figure 3 shows that there is a significant vacancy-Ni attraction in the MGS, which is strongest around 5%Ni. According to our EIM, the MGS remains antiferromagnetic up to 5%Ni, above which the reduced magnetization starts to increase. Therefore, the maximum $G_b^{V\text{-}A}$ occurs around 5%Ni, that is, the highest Ni concentration in the strictly antiferromagnetic Fe lattice.

As a further confirmation, we calculate the binding energy between a vacancy and a Ni cluster in the AFD Fe using our EIM and DFT. The binding energy E_b is calculated as the energy difference between the system with the vacancy and the Ni cluster far away from each other, and the system with the two at the 1NN distance. Hence a positive E_b indicates an attraction. As shown in Fig. 4, both EIM and DFT confirm that E_b is positive and increases with increasing Ni cluster size. Therefore, in the presence of the attractive configurations, the jump frequencies to enter or exit such configurations have
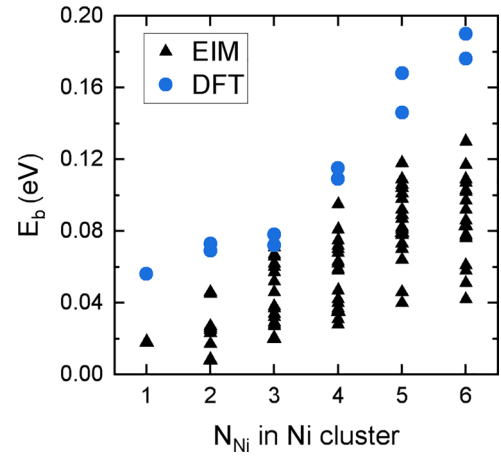
very different amplitudes, leading to strong kinetic correlations and low correlation factors.

D. Diffusion properties beyond equilibrium conditions

The present approach also enables us to evaluate diffusion-related quantities in nonequilibrium conditions, where a much larger amount of vacancies can be created, e.g., by a rapid quenching from high temperatures, by plastic deformation, or under irradiation [59]. In these cases, the diffusion coefficients are no longer functions of the equilibrium vacancy concentration. Meanwhile, the ratio of tracer diffusion coefficients D_{Fe}^*/D_{Ni}^* is a quantity independent of the vacancy concentration. It is a key parameter dictating the enrichment or depletion of an alloying element in sinks (e.g., grain boundaries) due to the so-called radiation-induced segregation (RIS), a frequently observed phenomenon under irradiation [60]. Figure 5(a) shows that D_{Fe}^*/D_{Ni}^* increases from 0.4 to 1 at 30%Ni, then it varies more slowly between 1 and 2, presenting a maximum around 60%Ni. Our prediction is in excellent
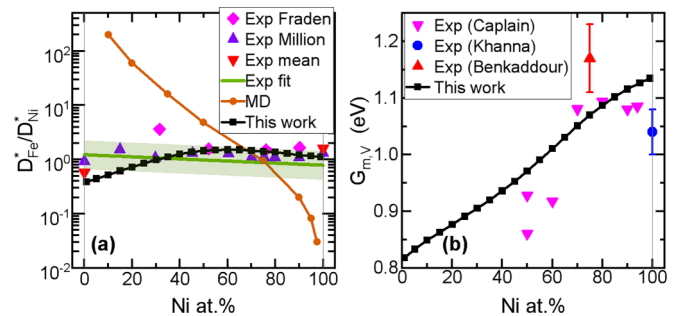

FIG. 5. Predicted (a) ratio between Fe and Ni tracer diffusion coefficients, and (b) vacancy migration magnetic free energy $G_{m,V}$ at 1223 K. In (a), the experimental ratios are computed using data of D^* compiled in Ref. [38] (diamonds and up-triangles use data from [55] and [38], respectively; down-triangles use the mean D^* of Fe and Ni; the solid line uses D^* linearly fitted to all the compiled experimental data; the shaded area indicates the error bars); classical MD results are from Ref. [42]. In (b), the experimental vacancy migration energies are taken from Refs. [56–58].

TABLE II. Magnetic and nonmagnetic on-site parameters for the SP atom.

	A_{SP} (meV/μ_B^2)	B_{SP} (meV/μ_B^4)	ϵ_{SP} (meV)
SP = Fe	−205.2016	15.6446	−7707.2197
SP = Ni	74.0210	301.1836	−5883.8414

TABLE III. Magnetic exchange interaction parameters $J_{SP,OL}$ (in meV/μ_B^2) between the SP atom and the OL atom separated by a given distance.

SP	OL	1NN	2NN	3NN	4NN
Fe	Fe	−5.3855	−8.0161	1.5916	−0.6457
Fe	Ni	−24.5305	5.8653	9.1694	−9.4957
Ni	Ni	−71.6976	−35.0767	13.9183	−8.3676
Ni	Fe	−13.2241	−3.7589	−18.7414	5.8729

agreement with experimental data above 30%Ni, whereas it is lower than the experimental ratios by a factor of 2 in the Fe-rich limit, in which the experimental data show a larger dispersion. To the best of our knowledge, the only previous theoretical determination of these ratios comes from classical MD simulations [42] (Fig. 5). However, those results strongly deviate from our predicted values and the experimental ones. Such a deviation suggests a high sensitivity of these ratios to the quality of the empirical potentials used. Our results suggest that the coefficient ratios in fcc Fe-Ni alloys may actually be different from those in fcc Fe-Ni-Cr alloys. For the latter, previous experiments [61] in the alloys with 20–45 %Ni found the D^*_{Fe}/D^*_{Ni} to be 1.8, while existing models addressing the RIS usually assumed the ratio to be rather large (larger than 2 or 3).

It is also relevant to determine vacancy migration energies and compare them with available experimental data, since they control physical processes such as the growth rate of dislocation loops under irradiation [62,63]. In fcc Fe-Ni alloys, there are available experimental values from magnetic anisotropy [56] and electrical resistivity measurements [57], and the ones extrapolated from the electrical resistivity results in Fe-Ni-Cr alloys with varying Cr content [58]. We have determined the vacancy migration magnetic free energy $G_{m,V}$ with effects of magnetic excitations included (Appendix B). We find a good theoretical-experimental agreement as shown in Fig. 5(b), where we predict a nearly linear increase in $G_{m,V}$ from pure Fe to pure Ni.

IV. CONCLUSION

In summary, we propose a DFT-based modeling approach and apply it to the prediction of atomic diffusion properties in PM fcc Fe-Ni alloys as a function of composition. It consists in kinetic Monte Carlo simulations coupled with an effective interaction model entirely parametrized on DFT. Both chemical and magnetic variables and their coupling are explicitly taken into account. The accuracy of our approach is attested by the good modeling-experiment agreement in various diffusion-related quantities. In addition, we also propose a way to express the tracer diffusion coefficient in concentrated alloys in terms of its constituents using the same formal expression as in the dilute case.

For PM Fe-Ni alloys, we predict a weak composition dependence of the diffusion coefficients, which can be explained by the interplay of the stronger but distinct composition dependence of the equilibrium vacancy concentration and the effective jump frequency.

Regarding the impact of magnetic disorder, we find a much stronger composition dependence of the diffusion properties if we assume the 0 K magnetic configurations instead of the

PM state. Such a reduction of the chemical-interaction effect due to magnetic disorder was evidenced in some dilute bcc Fe alloys. Here we find the same effect well beyond the dilute limit, regardless of the alloy concentration. The distinct diffusion properties between the ordered and disordered magnetic states also indicate that the magnetic ground state is not a good representation for the modeling of diffusion in the PM concentrated alloys.

Finally, the present model provides a way to access the diffusion data for a broad range of temperatures, complementing nicely the diffusion experiments feasible only at high temperatures. It is fully transferable to other concentrated magnetic metal alloys under both equilibrium and nonequilibrium conditions.

APPENDIX A: MODEL PARAMETERS

The numerical values of the parameters in the expression of E_{SP} [Eq. (3)] parametrized in this work are given in Tables II–IV. The parameters for the on-lattice configuration (E_{OL}) can be found in Ref. [36].

APPENDIX B: COMPUTATION OF VACANCY EFFECTIVE MIGRATION FREE ENERGY

In the following, we describe how the vacancy effective migration free energy $G_{m,V}$ shown in Fig. 5(b) is computed in MC simulations. We start with the attempt frequency of the

TABLE IV. Nonmagnetic pair interaction parameters $V_{SP,OL}$ (in meV) between the SP atom and the OL atom separated by a given distance.

SP	OL	1NN	2NN	3NN	4NN
Fe	Fe	−28.7755	47.2913	30.9704	−29.1062
Fe	Ni	−34.6618	14.367	62.7312	−19.1265
Ni	Ni	147.0236	54.6353	57.2937	−56.6513
Ni	Fe	65.3323	12.8306	60.7932	−67.5517

vacancy and then relate it to the vacancy jump frequency and finally $G_{m,V}$. As the vacancy exchanges with both Fe and Ni atoms, the attempt frequency of the vacancy is no longer a constant but relates to $\Gamma_{0,Fe}$ and $\Gamma_{0,Ni}$ as follows [24]:

$$\Gamma_{0,V}^i = z_{Fe}^i \Gamma_{0,Fe} + z_{Ni}^i \Gamma_{0,Ni}, \tag{B1}$$

where z_{Fe}^i and z_{Ni}^i are the numbers of 1NN Fe and Ni atoms for a given local chemical environment i.

We define an effective attempt frequency $\Gamma_{0,V}$ using the average number of 1NN Fe and Ni atoms (z_{Fe} and z_{Ni}) around a vacancy:

$$\Gamma_{0,V} = z_{Fe} \Gamma_{0,Fe} + z_{Ni} \Gamma_{0,Ni}. \tag{B2}$$

On the other hand, the effective jump frequency of the vacancy is simply equal to the total number of atomic jumps N_{jump} divided by the time interval t_{MC}:

$$\Gamma_V = \frac{N_{jump}}{t_{MC}}. \tag{B3}$$

Then, similar to Eq. (13), we have

$$\Gamma_V = \Gamma_{0,V} \exp\left(-\frac{G_{m,V}}{k_B T}\right). \tag{B4}$$

Therefore, vacancy migration magnetic free energy can be calculated as

$$G_{m,V} = -k_B T \ln \frac{\Gamma_V}{\Gamma_{0,V}}. \tag{B5}$$

[1] M. Y. Lavrentiev, R. Drautz, D. Nguyen-Manh, T. P. C. Klaver, and S. L. Dudarev, Phys. Rev. B **75**, 014208 (2007).

[2] M. Ekholm, H. Zapolsky, A. V. Ruban, I. Vernyhora, D. Ledue, and I. A. Abrikosov, Phys. Rev. Lett. **105**, 167208 (2010).

[3] F. Körmann, T. Hickel, and J. Neugebauer, Curr. Opin. Solid State Mater. Sci. **20**, 77 (2016).

[4] I. Abrikosov, A. Ponomareva, P. Steneteg, S. Barannikova, and B. Alling, Curr. Opin. Solid State Mater. Sci. **20**, 85 (2016).

[5] Y. Iijima, J. Phase Equilib. Diff. **26**, 466 (2005).

[6] O. Senninger, E. Martínez, F. Soisson, M. Nastar, and Y. Bréchet, Acta Mater. **73**, 97 (2014).

[7] F. Körmann, A. A. H. Breidi, S. L. Dudarev, N. Dupin, G. Ghosh, T. Hickel, P. Korzhavyi, J. A. Muñoz, and I. Ohnuma, Phys. Status Solidi B **251**, 53 (2014).

[8] I. Stockem, A. Bergman, A. Glensk, T. Hickel, F. Körmann, B. Grabowski, J. Neugebauer, and B. Alling, Phys. Rev. Lett. **121**, 125902 (2018).

[9] O. Senninger, F. Soisson, E. Martínez, M. Nastar, C.-C. Fu, and Y. Bréchet, Acta Mater. **103**, 1 (2016).

[10] A. J. Ardell and P. Bellon, Curr. Opin. Solid State Mater. Sci. **20**, 115 (2016).

[11] M. Athènes, P. Bellon, G. Martin, and F. Haider, Acta Mater. **44**, 4739 (1996).

[12] H. Mehrer, *Diffusion in Solids*, Springer Series in Solid-State Sciences Vol. 155 (Springer, Berlin, 2007), pp. 1–246.

[13] J. Liu, L. J. Riddiford, C. Floristean, F. Goncalves-Neto, M. Rezaeeyazdi, L. H. Lewis, and K. Barmak, J. Alloys Compd. **689**, 593 (2016).

[14] F. Soisson, A. Barbu, and G. Martin, Acta Mater. **44**, 3789 (1996).

[15] F. Soisson and C.-C. Fu, Phys. Rev. B **76**, 214102 (2007).

[16] M. Nastar and F. Soisson, Phys. Rev. B **86**, 220102(R) (2012).

[17] D. R. Alfonso and D. N. Tafen, J. Phys. Chem. C **119**, 11809 (2015).

[18] S. Mahmoud and N. Mousseau, Materialia **4**, 575 (2018).

[19] S. L. Thomas and S. Patala, Acta Mater. **196**, 144 (2020).

[20] A. Roy, J. Munshi, and G. Balasubramanian, Intermetallics **131**, 107106 (2021).

[21] A. D. Leclaire and A. B. Lidiard, Philos. Mag. **1**, 518 (1956).

[22] A. D. Leclaire, J. Nucl. Mater. **69-70**, 70 (1978).

[23] J. R. Manning, Phys. Rev. **136**, A1758 (1964).

[24] J. R. Manning, Phys. Rev. B **4**, 1111 (1971).

[25] A. R. Allnatt and A. B. Lidiard, *Atomic Transport in Solids* (Cambridge University Press, Cambridge, 1993).

[26] J. D. Tucker, R. Najafabadi, T. R. Allen, and D. Morgan, J. Nucl. Mater. **405**, 216 (2010).

[27] T. Schuler and M. Nastar, Phys. Rev. B **93**, 224101 (2016).

[28] T. Schuler, L. Messina, and M. Nastar, Comput. Mater. Sci. **172**, 109191 (2020).

[29] S. Huang, D. L. Worthington, M. Asta, V. Ozolins, G. Ghosh, and P. K. Liaw, Acta Mater. **58**, 1982 (2010).

[30] H. Ding, V. I. Razumovskiy, and M. Asta, Acta Mater. **70**, 130 (2014).

[31] O. Hegde, V. Kulitckii, A. Schneider, F. Soisson, T. Hickel, J. Neugebauer, G. Wilde, S. Divinski, and C.-C. Fu, Phys. Rev. B **104**, 184107 (2021).

[32] A. Schneider, C. C. Fu, F. Soisson, and C. Barreteau, Phys. Rev. Lett. **124**, 215901 (2020).

[33] A. Schneider, C.-C. Fu, O. Waseda, C. Barreteau, and T. Hickel, Phys. Rev. B **103**, 024421 (2021).

[34] H. Wen and C. H. Woo, J. Nucl. Mater. **455**, 31 (2014).

[35] H. Wen and C. H. Woo, J. Nucl. Mater. **470**, 102 (2016).

[36] K. Li, C.-C. Fu, M. Nastar, F. Soisson, and M. Y. Lavrentiev, Phys. Rev. B **106**, 024106 (2022).

[37] P.-W. Ma and S. L. Dudarev, *Handbook of Materials Modeling* (Springer International, Cham, 2020), pp. 1017–1035.

[38] B. Million, J. Růžičková, J. Velíšek, and J. Vřešťál, Mater. Sci. Eng. **50**, 43 (1981).

[39] B. Jonsson, Scand. J. Metall. **23**, 201 (1994).

[40] S. Zhao, G. M. Stocks, and Y. Zhang, Phys. Chem. Chem. Phys. **18**, 24043 (2016).

[41] S. Zhao, Y. Osetsky, and Y. Zhang, J. Alloys Compd. **805**, 1175 (2019).

[42] Y. N. Osetsky, L. K. Béland, A. V. Barashev, and Y. Zhang, Curr. Opin. Solid State Mater. Sci. **22**, 65 (2018).

[43] K. Ferasat, Y. N. Osetsky, A. V. Barashev, Y. Zhang, Z. Yao, and L. K. Béland, J. Chem. Phys. **153**, 074109 (2020).

[44] Y. Osetsky, A. V. Barashev, and Y. Zhang, Curr. Opin. Solid State Mater. Sci. **25**, 100961 (2021).

[45] K. Li, C.-C. Fu, and A. Schneider, Phys. Rev. B **104**, 104406 (2021).

[46] K. Li and C.-C. Fu, Phys. Rev. Mater. **4**, 023606 (2020).

[47] K. Li, Magnetochemical coupling effects on thermodynamics, point-defect formation and diffusion in Fe-Ni alloys: A theoretical study, Ph.D. thesis, Université Paris–Saclay (2021).

[48] H. Wen, P.-W. Ma, and C. Woo, J. Nucl. Mater. **440**, 428 (2013).

[49] I. Novikov, B. Grabowski, F. Körmann, and A. Shapeev, npj Comput. Mater. **8**, 13 (2022).

[50] J. Crangle and G. C. Hallam, Proc. R. Soc. A **272**, 119 (1963).

[51] M. Peschard, Rev. Métallurg. **22**, 490 (1925).

[52] J. M. Cowley, Phys. Rev. **77**, 669 (1950).

[53] J. M. Cowley, Phys. Rev. **138**, A1384 (1965).

[54] L. Ruch, D. R. Sain, H. L. Yeh, and L. Girifalco, Solid State Commun. **18**, vi (1976).

[55] F. Fraden, B.S. thesis, Massachusetts Institute of Technology, 1963.

[56] A. Caplain and W. Chambron, Acta Metall. **25**, 1001 (1977).

[57] S. K. Khanna and K. Sonnenberg, Radiat. Eff. **59**, 91 (1981).

[58] A. Benkaddour, C. Dimitrov, and O. Dimitrov, J. Nucl. Mater. **217**, 118 (1994).

[59] H. Ullmaier, P. Ehrhart, P. Jung, and H. Schultz, *Atomic Defects in Metals*, edited by H. Ullmaier, Landolt-Börnstein–Group III, Condensed Matter Vol. 25 (Springer-Verlag, Berlin, 1991).

[60] M. Nastar and F. Soisson, *Comprehensive Nuclear Materials*, 2nd ed. (Elsevier, Amsterdam, 2020), Vol. 1, pp. 235–264.

[61] S. J. Rothman, L. J. Nowicki, and G. E. Murch, J. Phys. F **10**, 383 (1980).

[62] Y. Abe, Y. Satoh, and N. Hashimoto, Philos. Mag. **102**, 1173 (2022).

[63] A. Hardouin Duparc, C. Moingeon, N. S. de Grande, and A. Barbu, J. Nucl. Mater. **302**, 143 (2002).